THE ASTROPHYSICAL JOURNAL, 512:901–915, 1999 February 20

HUBBLE SPACE TELESCOPE FAINT OBJECT SPECTROGRAPH OPTICAL AND ULTRAVIOLET SPECTROSCOPY OF THE BOW SHOCK HH 47A[1]

PATRICK HARTIGAN,[2] JON A. MORSE,[3] JASON TUMLINSON,[3] JOHN RAYMOND,[4] AND STEVE HEATHCOTE[5]
Received 1998 April 16; accepted 1998 September 22

ABSTRACT

We present new spectra obtained with the Faint Object Spectrograph aboard the *Hubble Space Telescope* of the HH 47A bow shock and Mach disk that cover the entire spectral range between $\lambda\lambda$2220 and 6810. In addition to emission lines seen previously from HH objects, we uncover over a dozen weak Fe II transitions in the ultraviolet. The flux ratios between these permitted lines can only be understood if transitions to the ground state are resonantly scattered within HH 47A. The expected column density of Fe II within HH 47A suffices to scatter these lines, although the scattering optical depths imply that the Fe II line broadening must exceed that expected from thermal motions. Excitation of ultraviolet Fe II occurs locally within HH 47A, probably from collisions within the hot postshock gas and not from UV pumping from some nearby O stars. The data show no evidence for significant depletion of Fe within HH 47A. The emission line's fluxes and ratios indicate that jet material currently enters the Mach disk with a density of ~ 350 cm^{-3} and a velocity of ~ 40 km s^{-1}. The mass-loss rate of the exciting star, as measured by the mass flux through the Mach disk, is $1.6 \times 10^{-8}\ M_{\odot}$ yr^{-1}. This mass-loss rate is considerably lower than that closer to the star where the jet is brighter, probably because the density along the jet is highly nonuniform. A single-shock velocity does not match the bow shock spectrum well. We propose that secondary shocks reheat the gas within the cooling zone of the HH 47A bow shock. Compression from the first shock will cause these secondary shocks to be strongly magnetized, and the secondary shocks should emit strongly in low-excitation lines such as Mg II, C II], and [S II]. The weak blue continua seen at optical wavelengths in spectra of the Mach disk and bow shock extend into the ultraviolet and have spectral energy distributions and total fluxes consistent with those expected from two-photon emission.

Subject headings: accretion, accretion disks — ISM: jets and outflows — shock waves — stars: individual (HH 47A) — stars: pre–main-sequence

1. INTRODUCTION

Emission-line spectroscopy of the cooling regions behind shock fronts is one of the best ways to understand the dynamics of astrophysical flows. Analysis of radiation from shocked regions constrains a wide range of physical parameters within the shocks, including the density, shock velocity, abundances, and in some cases even the magnetic field strength. Often it is possible to observe distinct ionization zones within the gas as it cools, and in some cases collisional excitation of neutral atoms at the shock front not only marks the physical location of the shock wave but also gives clues to the plasma processes that operate there.

Shocks that lack a strong external photoionizing source are somewhat simpler to study than their photoionized counterparts. Two types of emission-line objects that usually lack strong external photoionizing sources are supernova remnants and HH objects. Detailed models of the emission lines from these objects have existed for some time (Raymond 1979; Dopita 1978) and have been reasonably successful at reproducing the observations. In the case of HH objects, which are shock fronts associated with outflows from accretion disks around young stars (Edwards, Mundt, & Ray 1993), emission-line images have resolved numerous cases of multiple bow shocks along stellar jets (Reipurth, Bally, & Devine 1997; Reipurth, Raga, & Heathcote 1992). Such images imply that many HH shocks form as fast material overtakes slower material in a nonsteady flow. In these cases, the "shock velocity," which to a large extent determines the emission lines present, equals the difference between the fast and slow velocities along the jet. When both proper-motion and radial velocity measurements exist, one can observe the true velocity of the flow with respect to the star, leading to a fairly complete overview of the system dynamics. In some objects both a bow shock, where slower material is accelerated and heated, and a Mach disk, where faster material is decelerated, are clearly visible (e.g., Reipurth & Heathcote 1991; Reipurth 1989). Such bow shock/Mach disk pairs are also present in numerical simulations (Stone & Norman 1993), although both shocks do not always exist in a nonsteady flow. Various types of fluid instabilities may also produce observable shocks in jets (e.g., Ray et al. 1996).

Despite the sometimes heavy reddening caused by the dusty environments of young stars, UV lines are particularly useful for studying HH objects because they probe a range of ionization states and involve permitted transitions that give information about scattering within the object. Blue continua that may be two-photon emission from H or from H_2 is best studied in the UV (Brugel, Shull, & Seab 1982; Dopita, Binette, & Schwartz 1982), and many lines of

[1] Based on observations made with the NASA *Hubble Space Telescope*, obtained at the Space Telescope Science Institute, which is operated by the Association of Universities for Research in Astronomy, Inc., under NASA contract NAS5-26555.

[2] Department of Space Physics and Astronomy, Rice University, 6100 South Main, Houston, TX 77005-1892.

[3] Center for Astrophysics and Space Astronomy, Campus Box 389, University of Colorado, Boulder, CO 80309.

[4] Harvard-Smithsonian Center for Astrophysics, MS 16, 60 Garden Street, Cambridge MA 02138.

[5] Cerro Tololo Inter-American Observatory, NOAO, Casilla 603, La Serena, Chile.

H_2 also appear in the ultraviolet (Schwartz 1983). Previous studies of HH objects with *IUE* (Böhm et al. 1987; Raymond, Hartigan, & Hartmann 1988), *Hubble Space Telescope* (*HST*; Curiel et al. 1995), and Hopkins Ultraviolet Telescope (HUT; Raymond, Blair, & Long 1997) have helped to clarify the shock velocities associated with these objects considerably.

In this paper we combine the results of the most sensitive spectroscopic study thus far undertaken for an HH object in the mid-ultraviolet (2200 Å $< \lambda <$ 3200 Å) with contemporaneous optical spectra taken with the same instrument. The object chosen was HH 47A, which exhibits a clearly defined bow shock and Mach disk at the end of a bright stellar jet (e.g., Heathcote et al. 1996). The jet has a spectacular morphology as it emerges from a dark globule isolated against the background emission of the Gum nebula (Dopita, Schwartz, & Evans 1982; Graham & Elias 1983). Both redshifted and blueshifted jets are visible, and multiple bow shocks are present in the blueshifted flow (Reipurth & Heathcote 1991; Hartigan, Raymond, & Meaburn 1990). The redshifted jet has evacuated an oblong cavity that is obscured by dust in the globule at optical wavelengths, but is well defined in the infrared (Eislöffel et al. 1994).

The most prominent bow shock within the blueshifted jet, HH 47A, has been studied extensively at optical wavelengths, but never in the mid-ultraviolet with high signal-to-noise ratio. Our new spectra reveal many faint permitted lines of Fe II that we use to investigate the radiative transfer within HH 47A. When combined with optical *HST* spectra we can constrain new shock models for HH 47A and understand more about the physical conditions within this system.

We describe the observations and data reduction procedures, including reddening corrections in § 2 and consider the ultraviolet Fe II lines in § 3. Shock models for the system appear in § 4, and our summary appears in § 5.

2. OBSERVATIONS AND DATA REDUCTION

We obtained spectra using the Faint Object Spectrograph (FOS) aboard *HST* on 1996 March 22 in ACCUM mode through the 0.″21 × 1.″71 slit imaged onto 1.″3 diodes. Two slit positions in HH 47A were observed, one located along the brightest portion of the bow shock emission and the other along the bright linear Hα feature that outlines the Mach disk. Both the Mach disk and bow shock positions were observed with gratings G570H, G400H, and G270H, to give a complete spectrum from $\lambda\lambda$2222 to 6818. Exposure times for the G570H, G400H, and G270H Mach disk spectra were 760, 720, and 850 s, respectively, whereas those for the bow shock were 1060, 1220, and 1480 s, respectively.

The locations of the slit on the sky appear superposed upon the WFPC2 image of Heathcote et al. (1996) in Figure 1. The position angle of the slit on the sky was 326.°9. Nonstellar sources can be difficult to position accurately within the FOS slit. We used a blind offset from a nearby star to the positions marked in Figure 1, where the coordinate offsets were found directly from the WFPC2 image, taking into account the proper motion of HH 47A (Eislöffel & Mundt 1994). To confirm that the offset moved the telescope to the correct position, we performed photometry on the WFPC2 [S II] image through an aperture the size of the FOS slit in a grid across HH 47A and compared the [S II] fluxes in the WFPC2 image with those in the FOS spectra. The position of the slit found in this manner was identical to the desired position to within 1 pixel on the WFPC2 ($\pm$0.″1). Changing the location of the slit by 1 pixel corresponds to about a 20% change in the total flux.

Data were initially reduced using the standard *HST* FOS pipeline in STSDAS and then reanalyzed using the best flat fields and inverse sensitivity functions available as of 1998 February. When dereddened according to a standard reddening law (Cardelli, Clayton, & Mathis 1988) with $A_V = 0.57$, which is the extinction Morse et al. (1994) found using the Balmer decrement of the background Gum nebula, both the bow shock and Mach disk spectra show very blue continua (Fig. 2, *top*). These continua appear unusual, as they are even more blue than expected from two-photon emission. An upturn in the reddest 500 Å of the G570H spectra of the Mach disk also appears odd and is probably instrumental. With the help of the FOS instrument scientists at STScI, we investigated possible instrumental effects in some detail.

There are several calibration uncertainties that can affect FOS spectra. Particularly worrisome is that the FOS scatters substantial amounts of visible light into the UV portions of the spectra. However, this only happens when a strong red continuum is present, which is not the case here. We also investigated the possibility that the anomalies arise from spectra whose centering on the diode array does not match that used to calibrate the sensitivity. This situation may occur for any extended object and is difficult to remove. However, this miscentering should only affect the extreme 100 Å or so and does not appear clearly in our data. Inaccurate dark count subtraction is another potential source of error. According to Figure 13 of Hayes & Lindner (1996), the standard pipeline reductions can underestimate the dark counts by as much as 30% for observations that have a high geomagnetic latitude (GML). Among our spectra, the two observations that had high geomagnetic latitudes, bow shock G270H and the Mach disk G570H spectra, also show the most anomalous continua.

Following this lead, we redid the dark subtractions for these data, increasing the dark for the G270H bow shock and G570H Mach disk spectra by 7% and 25%, respectively, as appropriate for the geomagnetic latitude of the observations. The results of this new dark subtraction appear in the middle panels of Figure 2. The anomalous red continuum in the Mach disk has now vanished, and although the bow shock continuum is still very blue, the new dark subtraction has reduced the flux in the bluest points by $\sim$20%, and the reddest continuum fluxes in the bow's G270H spectrum now match better with the bluest continuum fluxes in the G400H spectrum. The remaining residual continuum above that from two-photon emission in Figure 2 can be removed by using a lower reddening, $A_V = 0.30$, for HH 47A. This lower reddening was also used by Raymond et al. (1997) for the Vela supernova remnant.

To improve the wavelength solutions we obtained calibration exposures for each of the gratings while HH 47 was occulted by the Earth and used these instead of the generic files to convert diode number to wavelength. The spectral resolution $\lambda/\Delta\lambda$, as measured from the FWHM of the comparison lines, was $\sim$1400 for each wavelength setting, corresponding to a velocity resolution of about 210 km s^{-1}. The wavelength solutions determined from the $\sim$30 lines in the comparison spectra are quite good, with 1 σ errors of $\pm$7 km s^{-1}.

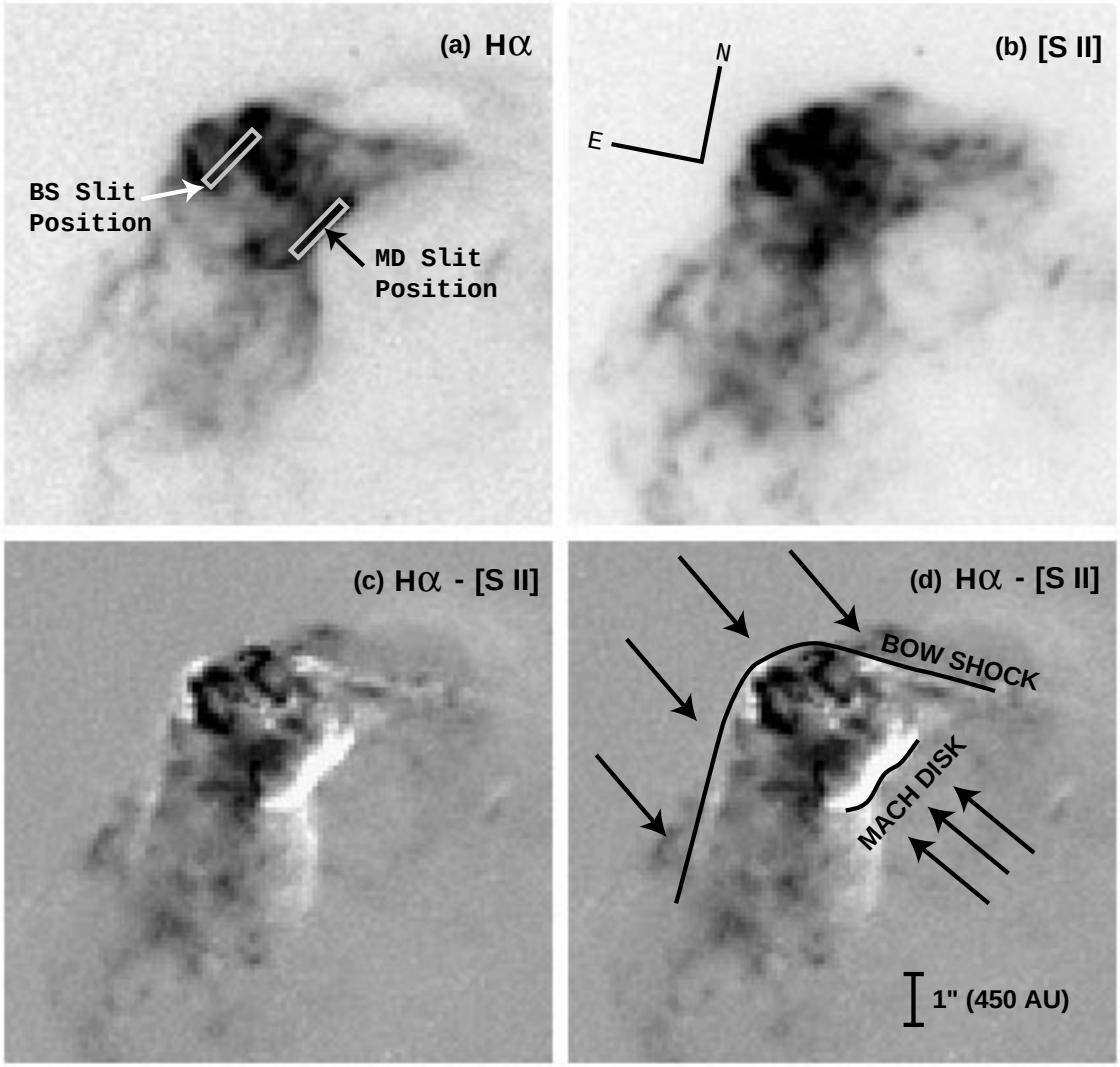

FIG. 1.—*Top: HST* images of HH 47A in Hα (*left*) and [S II] (*right*) taken from Heathcote et al. (1996). The FOS slit positions of the bow shock (BS) and Mach disk (MD) are shown superposed upon the Hα image. The directions north and east are shown. The position angle of the slit was 326°.9 for both the MD and BS observations. *Bottom:* The Hα-[S II] image of HH 47A from Heathcote et al. (1996), showing positions of the shock fronts as strong Hα emission. Arrows denote motion of the gas with respect to HH 47A, which itself moves away a young star located well off the lower right portion of the figure.

The velocity dispersion of the emitting gas within HH 47A is about 70 km s^{-1} (Morse et al. 1994; hereafter Mor94), considerably less than our spectral resolution, so the FOS data cannot resolve the line profile shapes. However, we do see that the spectra are clearly blueshifted. The observed heliocentric radial velocities of the brightest ($>5\ \sigma$) Mach disk and bow shock lines are -130 ± 42 and -100 ± 35 km s^{-1}, respectively, which compare well with the ground-based measurements of ~ -110 km s^{-1} (Mor94).

The observed line fluxes and wavelengths are compiled in Table 1, and the spectra of the bow shock and Mach disk appear in Figures 3–6. The spectra show lines predicted by models to occur in low-velocity shocks (e.g., Hartigan, Raymond, & Hartmann 1987), as well as dozens of Fe II lines that we discuss in detail in the next section.

3. ULTRAVIOLET Fe II EMISSION LINES IN LOW-VELOCITY SHOCKS

3.1. *Identification of the Observed Transitions*

Table 1 lists about a dozen Fe II lines that appear in the optical and a similar number in the UV spectra of HH 47A. The UV lines are all permitted transitions that occur as an electron decays from the $4p$ levels to the $4s$ levels. The optical lines are all forbidden transitions between the various multiplets of the $3d^6 4s$ electronic configuration. The optical lines have been seen before in HH 47A and in other HH objects (e.g., Böhm & Solf 1990) and are relatively easy to identify. The UV lines are more problematic to identify because there are hundreds of Fe II lines that may occur between $\lambda\lambda$2000 and 3000 (e.g., Fawcett 1988). To be confident that an identification is accurate we must be able to explain the presence or absence of other lines within the same multiplet.

We searched for emission-line objects that have been studied spectroscopically between $\lambda\lambda$2200 and 3000 in order to identify which Fe II transitions are likely to be strongest, but the strengths of these lines depend markedly upon density and the ambient radiation field. For example, the Fe II emission-line ratios of the symbiotic star RR Tel (Penston et al. 1983), those from chromospherically active stars like α Boo, α Tau, and β Gru (Judge & Jordan 1991), luminous blue variables (Szeifert et al. 1996; Zickgraf 1988), η Car (Viotti et al. 1989), and the supernova remnant

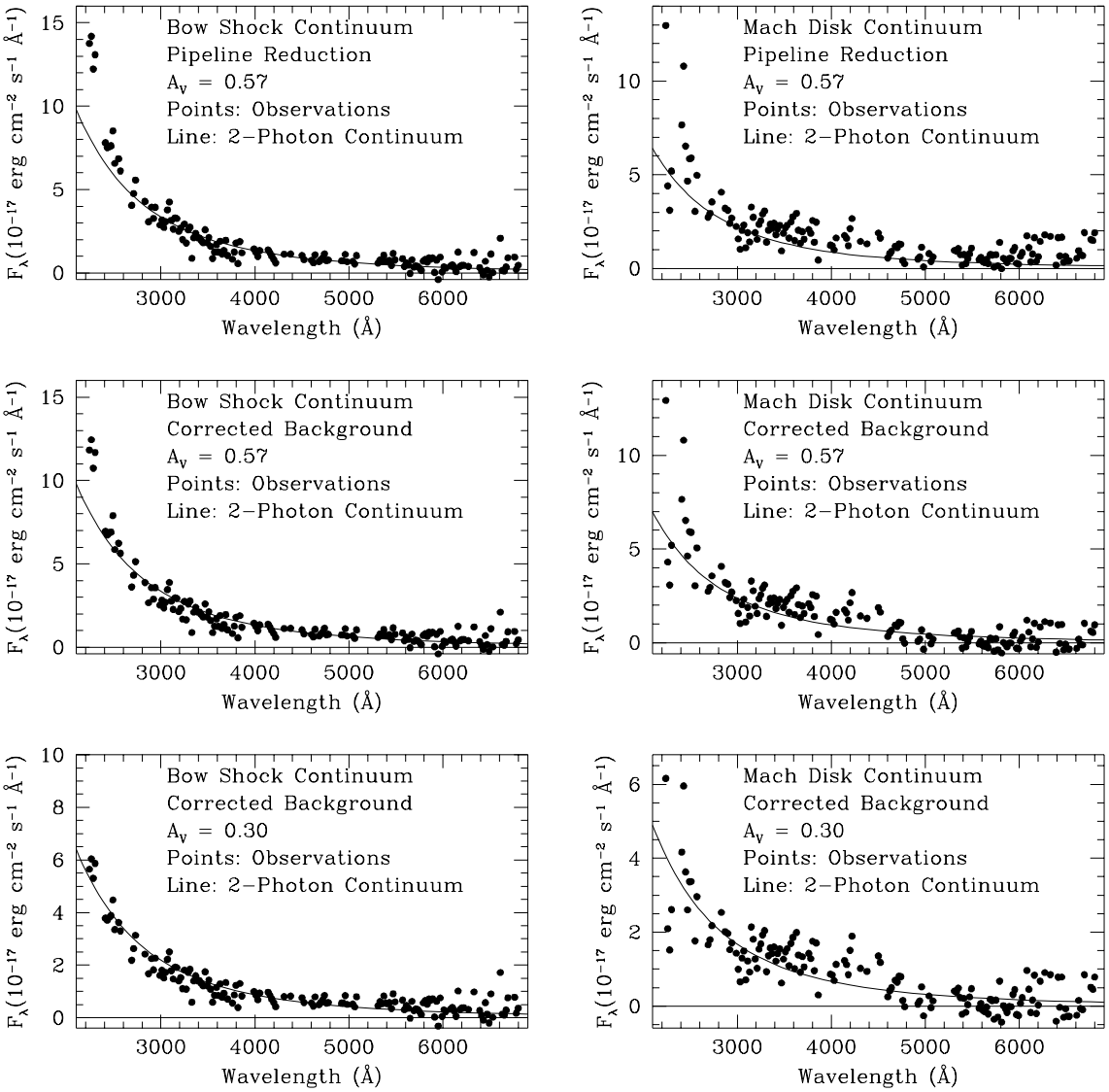

FIG. 2.—Measured and predicted continuum emission in the Mach disk (*right*) and bow shock spectra (*left*). The continuum points were each extracted from the data in 20 Å intervals devoid of emission lines. *Top:* Both spectra show a bright UV continuum whose spectrum is bluer than that expected from two-photon emission when reduced according to the standard pipeline and dereddened with $A_V = 0.57$. *Middle:* When the effects of high geomagnetic latitude are removed from the data, the blue continua become less striking and the anomalous red continuum in the Mach disk vanishes. *Bottom:* With correct dark count subtraction and a lower reddening, both the Mach disk and bow shock continua have shapes consistent with those expected from two-photon emission. The luminosity of the two-photon emission can be found from these plots and the bolometric corrections in Table 4.

N132D (Morse, Blair, & Raymond 1999) all differ markedly from the observed Fe II line ratios in HH 47A. Study of the resonance UV lines of Fe II can be quite instructive; for example, the absorption lines present in spectra of β Pic (Boggess et al. 1991) and 2 And (Cheng, Bruhweiler, & Neff 1997) have been used to infer the densities and temperatures of infalling material onto these stars.

To understand how ultraviolet Fe II lines behave in a low-density, shock-heated plasma like an HH object, we constructed the energy level diagram of Fe II shown in Figure 7. Levels are shown with their designations on the right and their energies above ground in cm^{-1} on the left. Each permitted transition marked by an arrow is labeled with the vacuum wavelength in angstroms, the Einstein A-value in s^{-1}, and the dereddened intensity of the line relative to Hβ = 100 listed between the brackets. If a "b" appears within the brackets it indicates that the line, if it exists, is blended with another line at the spectral resolution of the FOS. In the UV, the 2.5 σ detection limit for dereddened flux relative to Hβ = 100 is about 10. The Einstein A-values in Figure 7 were calculated from the latest oscillator strengths compiled by the "Fe Project" (Nahar 1995; Nahar & Pradhan 1994). The wavelengths were found from energy levels listed in Nahar (1995). The figure shows lines from each multiplet up to a level where no more lines are observed.

The first step in analyzing the Fe II lines is to check that the relative intensities for transitions that originate from the same upper level equals the ratio of the Einstein A-values for the two transitions. Two such pairs in the UV1 band, marked with asterisks in the figure, have detectable fluxes in both lines. Surprisingly, although the observed UV1 λ2612.65/λ2632.11 ratio of 1.25 $\pm$ 0.11 (1 σ error) is close to the expected value of 1.42, the observed UV1 λ2600.17/

TABLE 1

OBSERVED AND DEREDDENED EMISSION-LINE FLUXES[a]

LINE IDENTIFICATION[b]	BOW SHOCK			MACH DISK		
	Observed Wavelength	Observed Flux	Dereddened Flux[c]	Observed Wavelength	Observed Flux	Dereddened Flux[c]
Hβ Flux	...	6.4×10^{-16}	8.8×10^{-16}	...	8.0×10^{-16}	1.10×10^{-15}
C II] λ2326.9[d]	2325.73	405 (15)	616 (23)	2325.36	145 (10)	220 (15)
Si II] λ2335.1[d]	2333.87	48 (5)	73 (7)	...	...	...
Si II] λ2344.92 + Fe II (UV3) λ2344.21[e]	2344.06	47 (8)	70 (12)	...	...	...
Fe II (UV3) λ2365.55	2364.33	24 (5)	35 (7)	...	...	...
Fe II (UV2) λ2382.76 + Fe II (UV3) 2381.49[e]	2381.58	204 (15)	297 (22)	2381.55	72 (8)	105 (12)
Fe II (UV2) λ2396.36	2395.38	31 (5)	45 (7)	2395.73	21 (6)	30 (8)
Fe II (UV1) λ2600.17	2599.18	26 (5)	34 (7)	2598.89	20 (6)	26 (8)
Fe II (UV1) λ2612.65	2611.73	46 (7)	60 (9)	...	...	...
Fe II (UV1) λ2626.45	2625.34	190 (12)	245 (15)	2625.20	63 (5)	81 (6)
Fe II (UV1) λ2632.11	2631.32	37 (5)	48 (6)	...	...	...
[Al II] (1) λ2661.04	2659.82	15 (6)	19 (8)	...	...	...
Al II] (1) λ2669.89	2669.19	18 (6)	23 (8)	...	...	...
Fe II (UV63) λ2740.35	2739.82	15 (6)	19 (8)	...	...	...
Fe II (UV62) λ2750.13	2749.66	18 (6)	22 (8)	...	...	...
Fe II (UV62) λ2756.55	2755.44	18 (6)	22 (8)	...	...	...
Mg II λ2796.34	2795.33	1200 (30)	1483 (37)	2795.23	370 (10)	457 (12)
Mg II λ2803.52	2802.55	630 (15)	777 (19)	2802.48	205 (10)	253 (12)
C I]λ2968.1[d]	2966.88	65 (5)	78 (6)	2967.69	14 (4)	17 (5)
[O II] λ3728.5[d]	3728.40	107 (8)	118 (9)	3727.75	94 (5)	104 (6)
H8 λ3890.11	3889.78	10 (3)	11 (3)	...	...	...
Ca II λ3934.78	3934.29	86 (5)	94 (5)	3933.86	33 (4)	36 (4)
Ca II λ3969.59 + Hε λ3970.30	3968.89	74 (6)	80 (6)	3968.80	26 (5)	28 (5)
[S II] λ4069.71	4068.84	98 (10)	106 (11)	4068.36	23 (4)	25 (4)
[S II] λ4077.49	4077.11	17 (5)	18 (5)	4076.37	8 (3)	9 (3)
Hδ λ4102.85	4101.89	21 (5)	23 (5)	4102.09	25 (4)	27 (4)
[Fe II] (23F) 4115.63	4114.18	13 (5)	14 (5)	...	...	...
[Fe II] (21F) λ4245.17	4244.56	31 (5)	33 (5)	4245.08	17 (6)	19 (7)
[Fe II] (21F) λ4278.03	4277.12	9 (4)	10 (4)	...	...	...
[Fe II] (7F) λ4288.61	4287.73	38 (4)	40 (4)	...	...	...
Hγ λ4341.64	4341.63	40 (4)	42 (4)	4340.56	38 (5)	40 (5)
[Fe II] (7F) λ4360.56	4359.66	32 (5)	34 (5)	...	...	...
[Fe II] (6F) λ4417.51 + [Fe II] (7F) λ4415.02	4415.70	39 (4)	41 (4)	4414.36	14 (5)	15 (5)
[Fe II] (7F) λ4453.36	4451.23	15 (4)	16 (4)	...	...	...
[Fe II] (6F) λ4459.20	4457.80	10 (4)	11 (4)	...	...	...
[Mg I] λ4563.88	4562.98	20 (5)	21 (5)	...	...	...
Mg I] λ4572.37	4571.38	55 (5)	57 (5)	4572.76	22 (6)	23 (6)
[Fe II] (20F) λ4815.89	4814.13	14 (5)	14 (5)	...	...	...
Hβ λ4862.64	4861.84	100	100	4861.22	100	100
[Fe II] (20F) λ4890.99	4890.90	12 (5)	12 (5)	...	...	...
[Fe II] (19F) 5160.24	5159.17	55 (5)	54 (5)	5158.91	14 (6)	14 (6)
[N I] λ5200.5[d]	5199.23	213 (10)	208 (10)	5198.45	60 (6)	58 (6)
[Fe II] (19F) λ5263.07	5261.93	30 (5)	29 (5)	5260.52	15 (4)	15 (4)
[Fe II] (18F) λ5274.84	5272.82	10 (4)	10 (4)	...	...	...
[Fe II] (17F) λ5528.86	5527.91	13 (4)	12 (4)	...	...	...
[O I] λ6302.03	6299.75	560 (30)	515 (28)	6298.81	165 (15)	152 (14)
[O I] λ6365.53	6363.48	208 (15)	191 (14)	6361.53	53 (7)	49 (6)
Hα λ6564.56	6562.43	550 (25)	500 (23)	6561.79	435 (15)	395 (14)
[N II] λ6585.27	6584.09	95 (15)	86 (14)	6583.25	52 (12)	47 (11)
[S II] λ6718.26	6716.35	625 (20)	564 (18)	6714.70	165 (10)	149 (9)
[S II] λ6732.65	6730.67	810 (25)	730 (23)	6728.71	195 (10)	176 (9)
Two-photon continuum	...	...	18000 (2000)	...	...	10800 (2000)

[a] Flux measured through the 0.″2 × 1.″7 slit imaged onto 1.″3 diodes, in ergs cm^{-2} s^{-1}.
[b] Vacuum wavelengths.
[c] Dereddened with a standard galactic reddening curve, $A_V = 0.30$.
[d] Unresolved doublet or multiplet.
[e] Contribution of this line to the total flux is probably small—see text.

λ2626.45 ratio of 0.14 ± 0.01 is far from the predicted value of 4.54.

A closer look at the observed upper limits shows several line ratios that differ significantly from the ratios of the Einstein A-values. These ratios include the lack of the λ2586.65 line in the UV1 band, which should have a dereddened intensity of about 32 (observed $\lesssim$10) based on the fluxes and A-values of the other UV1 lines from the $z\ ^6D^o_{7/2}$

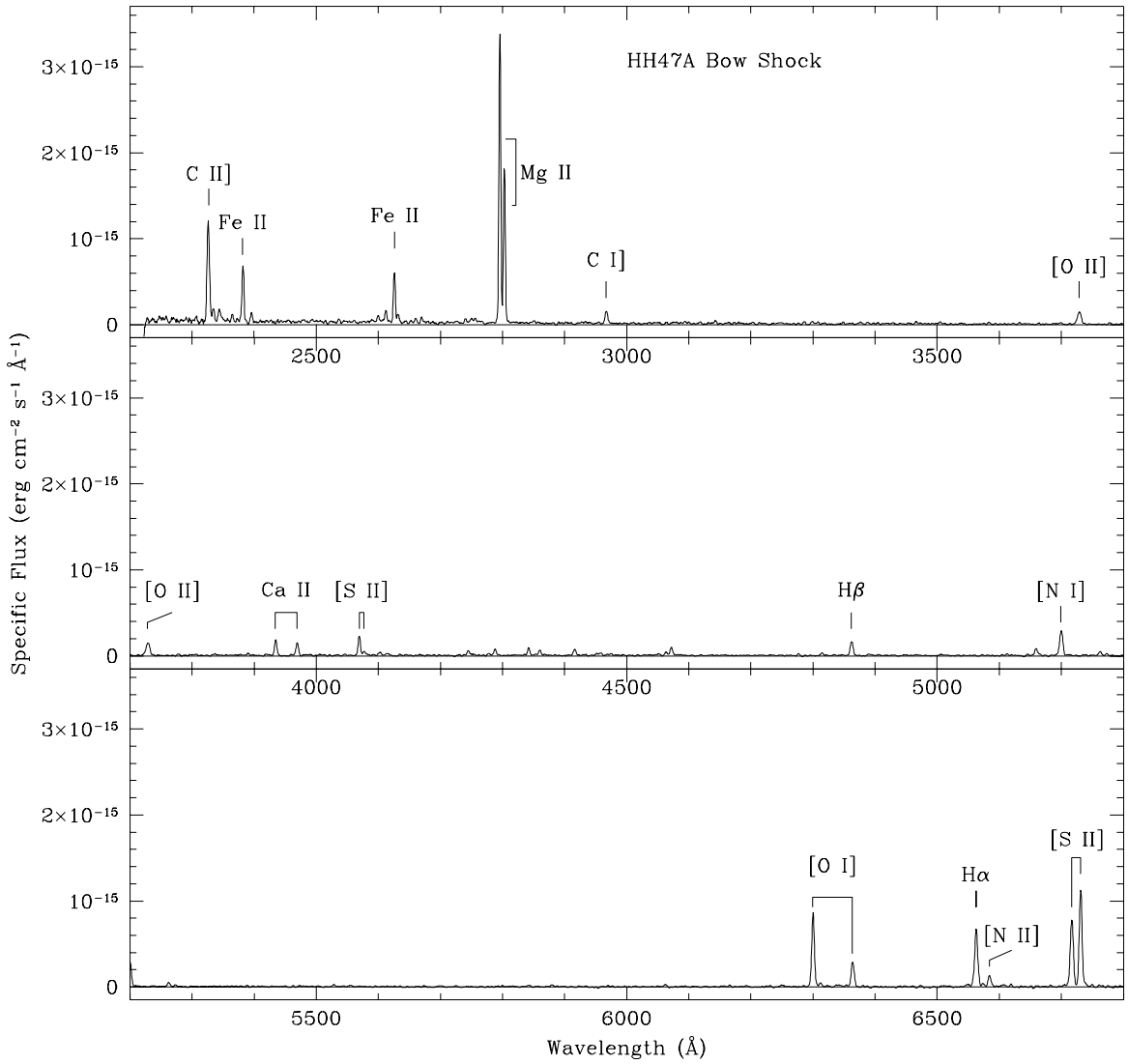

FIG. 3.—Spectrum of the bow shock of HH 47A, dereddened using $A_V = 0.30$. The Mg II λ2800 doublet is the strongest line in the spectrum.

level; the UV2 λ2374.46 transition, which should have a dereddened intensity of $\sim$11 (observed $\lesssim$10) based on the observed intensity of the UV2 λ2396.36 line; and the low intensity of the UV3 λ2344.21 line, which should have a dereddened intensity of 125 based on the observed intensity of the λ2365.55 line, but the UV3 line has an observed intensity of only 70, even though much of the observed flux probably comes from a blend with the Si II] λ2344.92 line (note the strong Si II] λ2335.1 feature). Lines that are consistent with the ratios of the A-values include the UV62 λ2717.50 line, which should have a dereddened intensity of $\sim$4 (observed $\lesssim$10) based on the observed intensity of the λ2750.13 line; and the UV63 λ2773.55 line, which should have a dereddened intensity of $\sim$3 (observed $\lesssim$10) based on the observed brightness of the λ2740.36 line.

Transitions from a common upper level whose ratios do not equal the ratios of the A-values share a common characteristic—*all transitions to the ground level, a* $^6D_{9/2}$*, are underluminous.* The easiest explanation for this phenomena is that transitions to the ground state are resonantly scattered from Fe II located within HH 47A or along the line of sight to it. In this regard, it is interesting that the *strongest* UV line of Fe II is the resonance UV2 line at λ2382.76 (the contribution of the UV3 λ2381.49 line to this blend should be in the noise based on the flux and A-value of the UV3 λ2365.55 line). The λ2382.76 line remains strong despite resonance scattering because unlike the other resonance transitions, the upper level $z^6F^o_{11/2}$ cannot decay within the multiplet by any other permitted transition.

Hence, we can explain the observed intensities of the dozen or so UV Fe II lines, *and* the lack of other Fe II lines in the same spectrum with a plasma that is optically thin in all transitions except for those that involve the ground state. In what follows we will use this information to infer how the Fe II becomes excited and to constrain the physical conditions within the Fe II scattering region.

3.2. *Resonance Lines and Column Densities*

As noted in the previous section, the observed UV1 λ2600.17/λ2626.45 ratio is a factor of 33 lower than that expected for an optically thin gas. We can use this factor to estimate the optical depth of scattering in these transitions. For this purpose we will denote energy levels $a^6D_{9/2}$, $a^6D_{7/2}$, and $z^6D_{9/2}$ as levels 1, 2, and 3, respectively. Hence, the λ2600.17 line represents the 3–1 transition, and the λ2626.45 line the 3–2 transition.

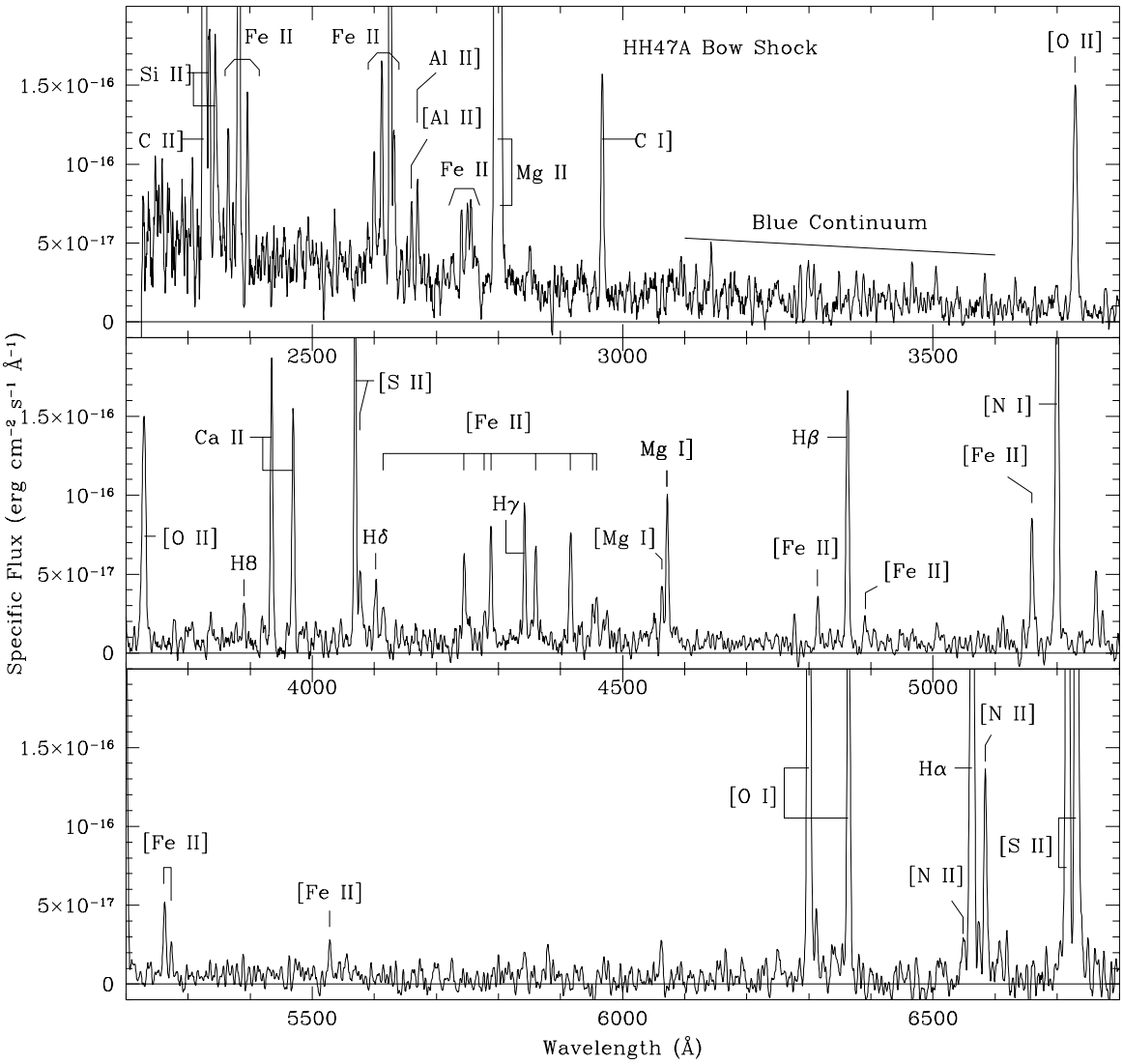

FIG. 4.—Same as Fig. 3 but scaled to show the fainter emission lines and blue continuum

The emergent intensity of a transition between energy levels 3 and 1 from a uniform slab of scattering optical depth τ_{13} is given by

$$I_{31}(\tau_{13}) = C_{31}(1 - e^{-\tau_{13}}) , \quad (1)$$

with

$$C_{31} = \frac{h\nu_{31} n_3 A_{31}}{4\pi n_1 \sigma_{13}} . \quad (2)$$

Here, A_{31} is the Einstein A-coefficient for the transition, n_i is the density in level i, ν_{31} is the frequency of the transition, and σ_{13} is the cross section for scattering from level 1 to level 3. Rewriting these equations for the 3–2 transition and taking the ratio we find

$$\frac{I_{31}(\tau_{13})}{I_{32}(\tau_{23})} = \frac{I_{31}(\tau_{13} = 0)}{I_{32}(\tau_{23} = 0)} \left[\left(\frac{\tau_{23}}{1 - e^{-\tau_{23}}} \right) \left(\frac{1 - e^{-\tau_{13}}}{\tau_{13}} \right) \right] , \quad (3)$$

where we have used the fact that in the optically thin limit

$$\frac{I_{31}(\tau_{13} = 0)}{I_{32}(\tau_{23} = 0)} = \frac{\nu_{31} A_{31}}{\nu_{32} A_{32}} . \quad (4)$$

To solve equation (3) for τ_{13}, we write

$$\frac{\tau_{13}}{\tau_{23}} = \frac{\sigma_{13}}{\sigma_{23}} \frac{n_1}{n_2} , \quad (5)$$

where

$$\frac{\sigma_{13}}{\sigma_{23}} = \left(\frac{g_2 A_{31}}{g_1 A_{32}} \right) \left(\frac{\lambda_{31}}{\lambda_{32}} \right)^2 = 3.56 \quad (6)$$

for the $\lambda\lambda$2600.17 and 2626.45 transitions. The calculation by Keenan et al. (1988) allows us to estimate the population of each of the levels in the $a\,^6D$ state as a function of temperature and electron density. For an electron density of 10^3 and $T \sim 10^4$ K, the ratio n_2/n_1 of the population of the $a\,^6D_{7/2}$ level to the $a\,^6D_{9/2}$ level is 0.015. Hence, $\tau_{2600} = 237\tau_{2626}$. Using this ratio in equation (3) we find $\tau_{2600} = 35$ and $\tau_{2626} = 0.15$.

Although lines that involve the ground level, $a\,^6D_{9/2}$, show evidence for resonant scattering, the same is not true of the first excited level, $a\,^6D_{7/2}$ (recall the observed fluxes of the UV1 line ratio λ2632.11/λ2612.65 agree with the ratios of the Einstein A-values). Hence, the $a\,^6D_{7/2}$ level must be

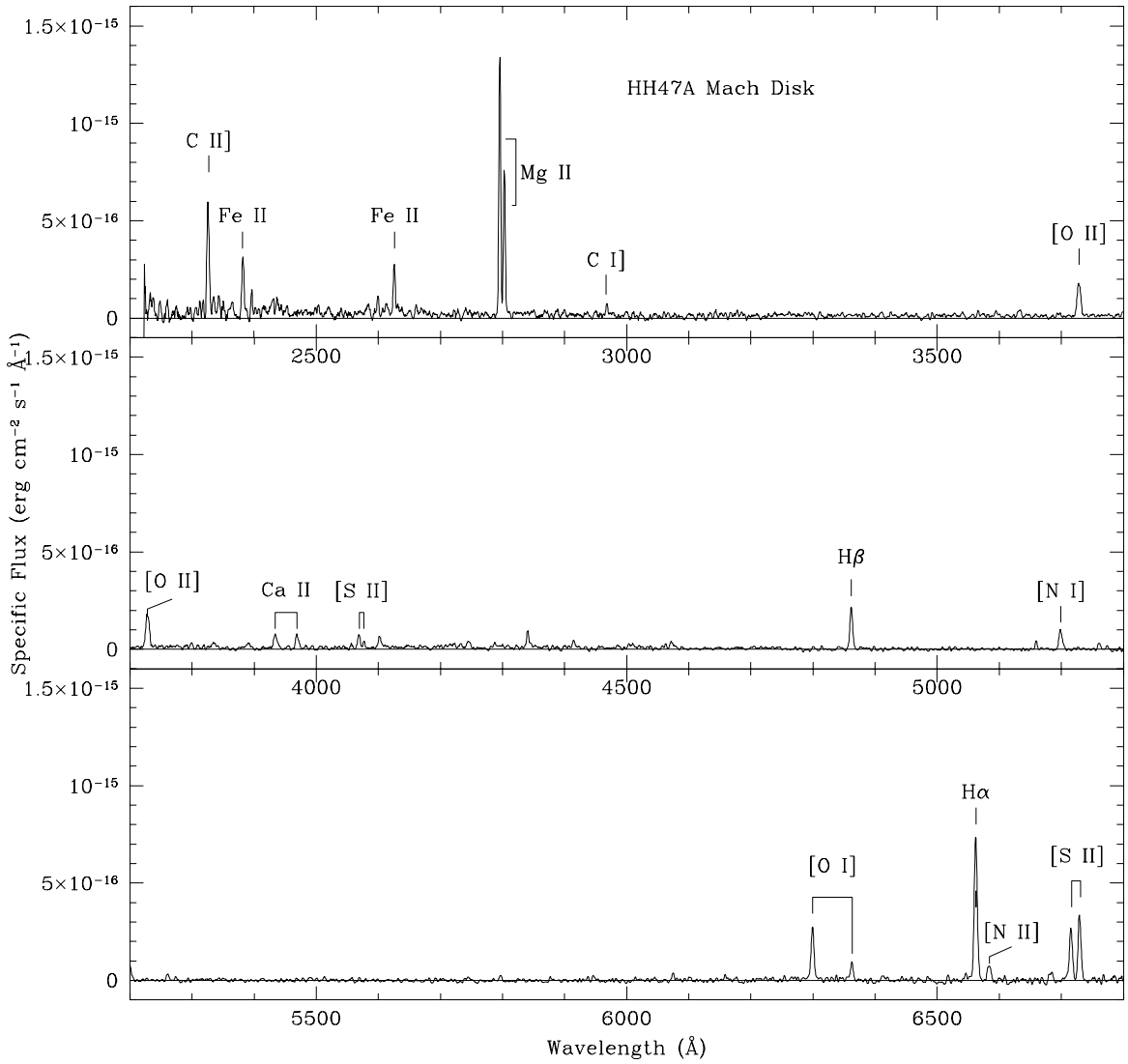

FIG. 5.—Same as Fig. 3 but for the Mach disk of HH 47A

optically thin to radiation. The optical depth of the $\lambda 2612.65$ line is $\tau_{2612} = 8.2 \times 10^{-3} \tau_{2600} = 0.29$, so that equation (3) implies

$$\frac{I_{2612}(\tau_{2612})}{I_{2632}(\tau_{2632})} = 1.42\left(\frac{1 - e^{-0.29}}{0.29}\right) = 1.23 , \qquad (7)$$

which agrees almost exactly with the observed ratio of 1.25 ± 0.11. These calculations show that the $\lambda 2612.65$ line is not heavily scattered.

As we calculated above, the optical depth over the profile of the $\lambda 2600$ Fe II line, measured from the total observed fluxes of the $\lambda\lambda 2600$ and 2626 lines, is ~ 35. This optical depth is actually an average over the unresolved line profile. For Gaussian broadening, we found that this average τ_{2600} is achieved when τ_{v_0}, the optical depth at line center, is about 90. The column density of Fe II is related to τ_{v_0} by the equation

$$\tau_{v_0} = N_{\text{Fe II}} \frac{\sqrt{\pi} e^2 f}{m_e c \Delta v} , \qquad (8)$$

where f is the oscillator strength and Δv is the line width.

To estimate $N_{\text{Fe II}}$ we take the emitting gas within the slit to extend $\sim 1''$, or $\sim 6.7 \times 10^{15}$cm, and the observed electron density in the emitting region to be $n_e \sim 10^3$ cm^{-3} in the bow shock of HH 47A (Mor94). We are interested in the density of Fe II within this region and so must estimate the total density n, which depends upon the ionization fraction of the material. Mor94 find the shock velocity of the HH 47A bow shock to be ~ 60 km s^{-1}, which implies an ionization fraction within the bow of about 20% (Hartigan, Morse, & Raymond 1994, their Fig. 16; note the ionization fraction is considerably lower than 20% within the jet). Hence $n \sim 5 \times 10^3$ cm^{-3}. If we assume Fe abundances from Allen (1973) and assuming all the Fe is Fe II, the density of Fe II is $n_{\text{FeII}} \sim 0.2$ cm^{-3}, and the column density $N_{\text{Fe II}}$ is about 1.3×10^{15} cm^{-2}.

For the $\lambda 2600$ transition of Fe II, $f = 0.24$, so

$$N = 1.07 \times 10^{12}\left(\frac{\Delta V}{1 \text{ km s}^{-1}}\right)\tau_{\lambda_0 = \lambda 2600} \text{ cm}^2 , \qquad (9)$$

where ΔV is the line broadening in km s^{-1}. Equation (9) shows that the column density of Fe II within HH 47A can make the $\lambda 2600.17$ line optically thick easily enough, with

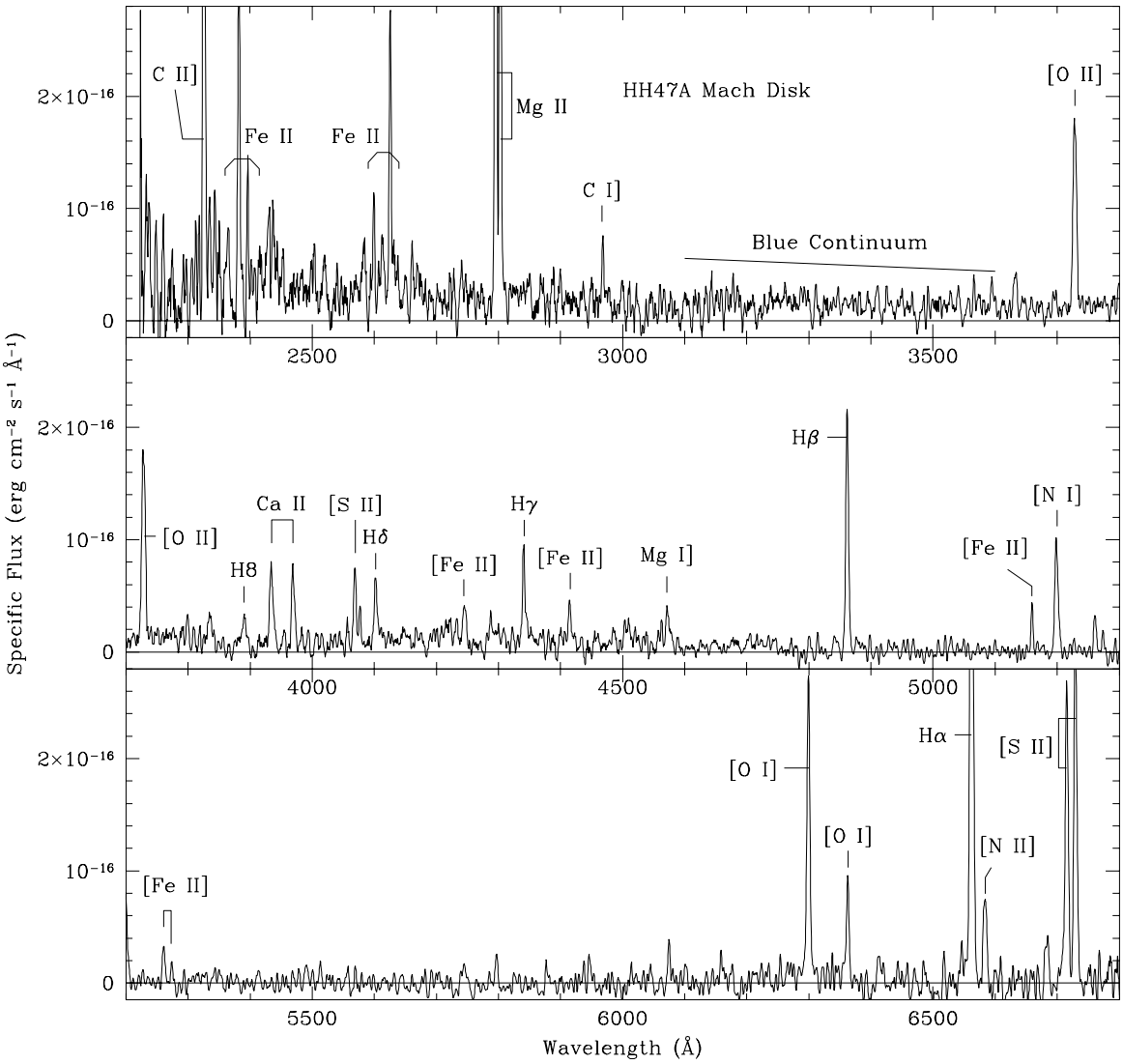

FIG. 6.—Same as Fig. 5 but scaled to show the fainter lines in the spectrum

$\tau_{v_0} \sim 90$ being achieved for $\Delta V \sim 14$ km s^{-1}. This velocity broadening exceeds that expected from thermal, ~ 1.7 km s^{-1} for Fe II at 10^4 K. The extra line width most likely arises from bulk motions within HH 47A as material is redirected by the bow shock.

Resonant scattering of the Fe II lines within HH 47A must occur locally. Although the intercloud medium also has sufficient column density to scatter the $\lambda 2600$ line (for $n \sim 0.1$ cm^{-3} through a total line of sight of 100 pc, the column density of Fe should be 1.2×10^{15} cm^{-2}), the Doppler shift of ~ -100 km s^{-1} of the emission lines from the HH object with respect to the ICM should effectively eliminate any such absorption. Note that we did not need to invoke any depletion of Fe onto grains to explain the scattering within HH 47A.

3.3. *Excitation of the UV* [Fe II] *Lines*

The most straightforward way to excite the Fe II atom ~ 5 eV to the $3d^6 4p$ states is to use 8 eV of the ~ 20 eV of collisional energy available per incident H atom in the 60–80 km s^{-1} shock that makes up HH 47A to singly ionize Fe, and the rest to collisionally excite the Fe II. It is possible that the preshock Fe is already ionized to Fe II by the ambient radiation field, so even less energy would be required for the collisional excitation.

However, HH 47A lies in a peculiar region for an HH object, close to the bright O stars ζ Pup and γ^2 Vel, so we should also consider whether or not this radiation may excite Fe II to the $3d^6 4p$ levels. The dereddened flux for the brightest permitted Fe II lines around $\lambda 2600$ in the bow shock spectrum is $\sim 10^{-15}$ ergs cm^{-2} s^{-1}. This flux originates from a $0''.2 \times 1''.3$ region, so the mean observed dereddened line intensity at the Earth is $\sim 1.6 \times 10^{-4}$ ergs cm^{-2} s^{-1} sr^{-1}. Hence, the emergent flux of the Fe II lines at the surface of the HH object is $F_{\rm HH} = 5.1 \times 10^{-3}$ ergs cm^{-2} s^{-1}. If the line is pumped by continuum UV from ζ Pup, then the UV flux from ζ Pup incident upon the HH object, integrated over the optically thick portion of the line profile, must equal $F_{\rm HH}$. At the Earth, the observed specific flux of ζ Pup at $\lambda 2600$ is 6.6×10^{-9} ergs cm^{-2} s^{-1} Å^{-1} (Longo et al. 1989). The distance of HH 47 from ζ Pup is probably about 100 pc, so the specific UV flux observed at the HH objects is $\sim 1.4 \times 10^{-7}$ ergs cm^{-2} s^{-1} Å^{-1} at $\lambda 2600$. The iron lines will absorb UV over ~ 15 km s^{-1}, or $\Delta\lambda \sim 0.13$ Å.

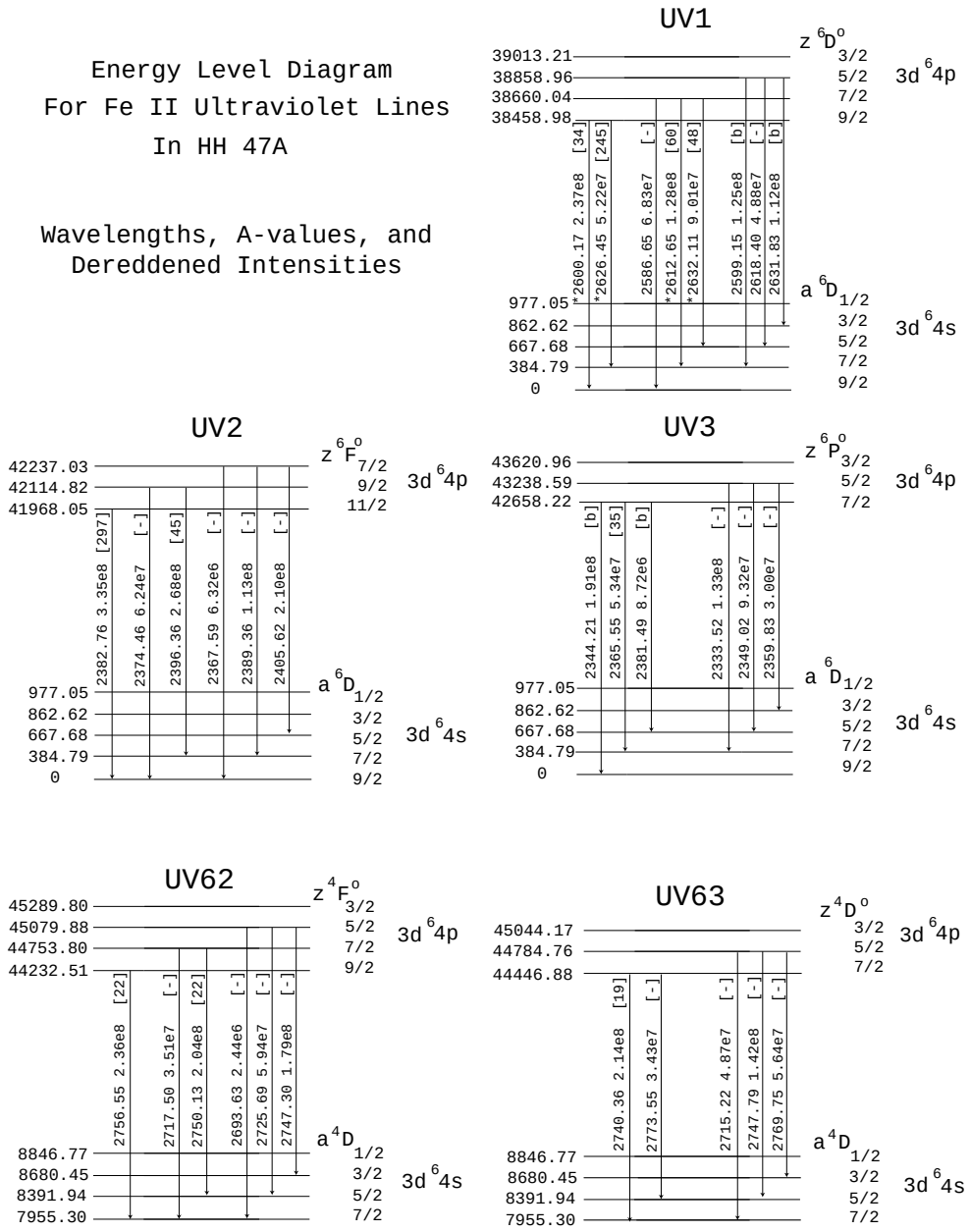

FIG. 7.—Energy level diagram for the observed UV transitions of Fe II. Designations appear to the right and energies above ground in cm^{-1} to the left of each level. Each transition is marked with the vacuum wavelength in angstroms, the Einstein A-value, and the observed intensity relative to Hβ. Further details are discussed in the text.

Thus, the incident UV flux from ζ Pup that may excite the Fe II transitions in HH 47 is $\sim 1.7 \times 10^{-8}$ ergs cm^{-2} s^{-1}, much less than the emergent F_{HH}.

We conclude that the excitation of Fe II is produced by collisional excitation within HH 47A. In other words, the observed ultraviolet Fe II lines do not result from the photoionized environment near HH 47, and as such should also be observable in other HH objects with sufficiently sensitive spectroscopy.

4. MODELS FOR THE EMISSION LINES AND BLUE CONTINUA

4.1. *Line Ratios, Fluxes, and Shock Models*

Mor94 derived shock parameters for HH 47A using ground-based optical Fabry-Perot and long-slit data. Although most of that analysis remains basically unchanged, one important point was not recognized until the *HST* images became available in 1995. In low ($\lesssim$100 km s^{-1}) velocity shocks the Hα/[S II] ratios generally increase with shock velocity, so Mor94 and Hartigan et al. (1993) interpreted regions with strong Hα as coming from high shock velocities. However, this is only true when we add emission from the entire cooling zone behind the shock. In the case of HH objects, cooling distances tend to be from 10 to 500 AU, a scale that is now resolved in *HST* images. The *HST* images make it clear that we observe Hα to have a high surface brightness with respect to [S II] wherever the shocks occur because much of the Hα comes from collisional excitation at the shock. With these considerations in mind, we now reexamine the physical parameters associated with the Mach disk (MD) and bow shock (BS) of HH 47A.

4.1.1. *The Mach Disk: Velocities and Densities*

The MD spectrum shows all the emission along the line of sight, including that from the Gum Nebula and from the wings of the bow shocks HH 47A and even the outer bow shock HH 47D (Fig. 1). To use this spectrum to analyze conditions in the Mach disk, we must isolate only those emission-line components that arise from the MD shock. Background contamination from the Gum Nebula will occur primarily in the Balmer lines, as metallic lines tend to be much brighter relative to Hβ in low-velocity shocks than they are in H II regions. Based on the relative fluxes of the Gum Nebula and the MD in the narrowband Hα images of Heathcote et al. (1996) the contamination of the MD and BS Balmer lines is less than 10%.

Correcting the MD spectrum for the superposed emission from the wings of the HH 47A and HH 47D bow shocks is more difficult. The [S II] *HST* images show clumpy emission that extends from the apex of the bow shock past the MD, and we cannot tell from our spectra what fraction of this is bow shock emission and what fraction true MD emission. A close examination of the sharp linear Hα feature in the *HST* images that marks the location of the MD shows that it also appears weakly in the [S II] images offset about 0.″15 in a direction toward the bow shock, which is where MD emission should occur. However, we cannot identify this [S II] feature with the MD with certainty because of the complexity of the overlapping umbrella of BS gas. If the linear [S II] feature is indeed postshock MD gas, the ratio of the fluxes of the sum of the red [S II] lines to Hα is $\sim$1.0. This observation gives a useful constraint on the shock velocity of the Mach disk, which we shall explore below.

We can also attempt to remove the contribution of the bow shock spectrum by subtracting a fraction of the BS spectrum from that of the MD. This procedure will only work to the degree that the spectrum in the wings of the bow, which are superposed upon the MD spectrum, resembles that near the apex, where the BS spectrum was taken. We found that all the high S/N metallic lines except [O II] λ3729 vanished in the MD spectrum when we subtracted the BS spectrum scaled by 0.4. The residual [O II] λ3727 emission may occur because this line is especially strong in the MD, or in the wings of HH 47A and HH 47D superposed upon the slit. It would be useful to verify that this line is bright in the MD because if so then the jet gas may be partially ionized (e.g., Hartigan et al. 1990).

4.1.2. *Mass-Loss Rates through the Mach Disk*

Methods for measuring mass-loss rates in young stars usually rely on emission-line luminosities of transitions such as [O I] λ6300 (e.g., Hartigan, Edwards, & Ghandour 1995). Systematic uncertainties in these estimates can be as high as 2 orders of magnitude because in T Tauri stars with unresolved jets it is often unclear how much of the radiating material fills the beam, what fraction of the flow does not radiate, and how many shocks exist within the beam. Mass-loss rates from resolved stellar jets should be more accurate, but uncertainties of factors of 3 remain common (see HMR94).

The dereddened Hα luminosity of the Mach disk is a direct measure of the mass-loss rate in the jet because about 30%–40% of the incident H atoms emit an Hα photon by collisional excitation. This percentage is independent of the preshock density and insensitive to the shock velocity (Chevalier & Raymond 1978; Chevalier, Kirshner, & Raymond 1980; Hartigan 1997). The dereddened Hα flux from the MD is 4.4×10^{-15} ergs cm^{-2} s^{-1}, so for a distance of 450 pc, the Hα luminosity of the MD is 1.1×10^{29} ergs s^{-1}. This luminosity must equal $\epsilon f n V_S A$, where ϵ is the energy of an Hα photon, $f \sim 0.4$ is the number of Hα photons per incident H atom into the MD, n is the preshock density of neutral H, V_S is the shock velocity in the MD, and $A \sim 6 \times 10^{31}$ cm^2 is the area of the MD.

To estimate the area A of the Mach disk we assumed that it is a disk of radius 0.″65, viewed on its edge, and so appears as a linear feature about 1.″3 in extent. If this estimate of A is incorrect, our values of n will change, but our value of the mass-loss rate will not, since this latter quantity depends only upon the observed luminosity of Hα, and the quantity f defined above. Hence, the rate that mass enters the MD is $\dot{M}_{\rm MD} = m_{\rm H} n V_S A = 2.4 \times 10^{-9}\ M_\odot$ yr^{-1}, so that $nV_S = 1.5 \times 10^4$ cm^{-3} km s^{-1}.

The mass-loss rate in the jet $\dot{M}_J$ is related to $\dot{M}_{\rm MD}$ by $\dot{M}_J = (V/V_S)\,\dot{M}_{\rm MD}$, where V is the velocity of the Mach disk with respect to the exciting star. Combining radial velocities of HH 47A measured by Mor94 and proper-motion measurements of Eislöffel & Mundt (1994; corrected to a distance of 450 pc) we obtain $V \sim 270$ km s^{-1}. In principle, the shock velocity could be anywhere from 10 km s^{-1}, the sound speed, up to 90 km s^{-1}, a limit imposed by the lack of high ionization lines such as [O III] in the spectrum. If we take the weak [S II] associated with the Mach disk as real, then $F([\text{S II}]\lambda6716 + [\text{S II}]\lambda6731)/F(\text{H}\alpha) \sim 1.0$. Using Figure 9 of Hartigan et al. (1994; hereafter HMR94), we find the shock velocity is 35–45 km s^{-1}. If one uses the above equations, this shock velocity implies that the mass-loss rate in the jet at the position of the MD is $1.6 \times 10^{-8}\ M_\odot$ yr^{-1}. This shock velocity also implies that $n = 350$ cm^{-3} in the jet before material enters the MD.

The mass-loss rate measured above is a factor of 20 lower than that found along the jet of HH 47 (HMR94). These different mass-loss rates can only be reconciled if material currently flows into the HH 47A Mach disk at a rate much lower than occurs closer to the star. But this behavior is exactly what is expected from a velocity variable flow—large bow shocks sweep up any slower gas and leave rarefied wakes (Stone & Norman 1993; Hartigan & Raymond 1993; Biro & Raga 1994). The result is that the flow becomes increasingly clumpy with age. This clumpiness is evident in HH 47A, where the jet is also considerably brighter closer to the star, and in fact is nearly invisible in the vicinity of the MD.

The ratio of mass accretion to mass outflow is a crucial parameter for many theoretical models of jet acceleration (e.g., Shu et al. 1995). Our results emphasize that when comparing mass outflow rates with mass accretion rates from young stars it is essential either to measure the mass outflow rate before the fluid dynamics clumps the flow into a few dense patches (i.e., as close to the star as possible), or to average the mass outflow rate over a section of the jet (as was attempted by HMR94).

4.1.3. *The Bow Shock: Shock Velocity, Density, and Magnetic Field*

Figure 1 shows that our slit position for the bow shock includes the brightest clumps near the apex of HH 47A. Although well defined, the HH 47A bow shock has some irregularities in its shape and intensity that can only be

modeled approximately by a planar shock model. Nevertheless, the exercise of fitting a model to the data is a useful one. The shock velocities and densities found by Mor94 are based in part on spatially resolved line profiles unavailable in the FOS data; these estimates provide a good starting point for our analysis, which our new data now extend to the UV.

Mor94 found a preshock density for the HH 47A bow shock of ~ 1000 cm^{-3} and the shock velocity of ~ 60 km s^{-1}. According to their model A060, the distances gas takes to cool to 10^4 and 10^3 K behind the shock are 1.1 and 131 AU, respectively, so our slit width of 90 AU should include most of the cooling zone behind any given shock. According to the diagnostic diagrams of HMR94, our optical line ratios imply a lower shock velocity of ~ 35 km s^{-1} (Table 2). If one uses the observed [S II] λ6716/[S II] λ6731 line ratio and Figure 19 of HMR94 for 30 km s^{-1} $\lesssim V_S \lesssim$ 40 km s^{-1}, the component of the preshock magnetic field parallel to the shock lies in the range 20 μG $\lesssim B_{\parallel} \lesssim$ 200 μG, consistent with the value used by Mor94. The preshock density, derived from the total Hβ flux, also agrees well the Mor94 value of ~ 1000 cm^{-3}.

TABLE 2

SHOCK VELOCITY ESTIMATES FOR THE HH 47A BOWSHOCK

Ratio	Figure[a]	Value	V_S (km s^{-1})[b]
[O I] λ6302/Hα	8	1.03	30
[S II] (λ6718 + λ6733)/Hα	9	2.59	31
[N I] λ5201/Hβ	10	2.08	31
[N II] λ6585/[O I] λ6302	11	0.17	38
[N I] λ5201/[N II] λ6585	12	2.42	37
[O II] λ3729/[OI] λ6300	13	0.23	40
Hα/Hβ	14	5.00	30

[a] Figure number from Hartigan et al. 1994 used to convert observed line ratio into estimate of the shock velocity.
[b] Shock velocity estimated from the line ratio.

After running several models where we attempted to fit both the Hβ flux and the relative forbidden line ratios, we settled on a 35 km s^{-1} shock model with a preshock density of 2500 cm^{-3} and a preshock magnetic field of 30 μG as being close to the best single-shock model. Results from this model appear alongside the observed line fluxes and ratios in Table 3. The main drawback of the single-shock model is that all of the forbidden line fluxes are too low compared with the observations. In particular, the [N II]/Hα ratio is only about half that observed. This ratio increases with shock velocity, but as the 60 km s^{-1} model line ratios show in Table 3, other low-excitation forbidden lines such as [O I] and [S II] get weaker relative to the Balmer lines as the shock velocity increases.

To address this problem we modeled a 60 km s^{-1} shock, as required by the emission-line profiles of Mor94, but with an additional weak shock that occurs after the gas has cooled for ~ 100 yr. The results are quite intriguing. Although the magnetic pressure is small compared with the ram pressure for the 60 km s^{-1} shock, by the time the gas cools for 100 yr the density, and hence the magnetic field, has increased by a factor of about 50. Because the magnetic pressure scales as B^2, any shock within the cooling region will encounter dense gas with a relatively large magnetic pressure, and a correspondingly low magnetosonic Mach number. The results from such a magnetized 40 km s^{-1} shock in Table 3 show very strong low-excitation lines, and in fact in all cases the observed line ratios listed in the last

TABLE 3

EMISSION-LINE MODELS FOR THE HH 47A BOWSHOCK

	Model[a]				
	I	II	III	IV	
	35	60	40	60/40	
	2500	200	10000	200/10000	
Line	30	20	1000	20/1000	Observed
Hβ flux[a]	9.6	8.1	1.3	9.4	8.8
C II] λ2327	130	30	1120	181	616
Si II] λ2335	14	3.1	107	17	73
Fe II UV1 lines	106	21	1580	237	387
Fe II UV2 lines	112	23	1570	237	342
Fe II UV3 lines	30	6.1	410	62	35
Mg II λ2800	457	74	4690	712	2260
[O II] λ3729	39	63	182	79	118
Ca II λ3935 + λ3970	84	8.5	4600	643	189
[S II] λ4070 + λ4077	52	7.6	558	84	124
Hβ λ4863	100	100	100	100	100
[N I] λ5200	90	8.3	2570	363	208
[O I] λ6302 + λ6366	393	53	7060	1022	706
Hα λ6565	442	332	536	360	500
[N II] λ6585	43	63	131	72	86
[S II] λ6718	271	48	6160	893	564
[S II] λ6733	364	58	7660	1109	730
Two-photon continuum	4600	1600	11700	3000	18000

NOTE.—The first row of units in the heading indicates the shock velocities of the models in units of km s^{-1}, the second row of units in the heading indicates the densities of the models in units of cm^{-3}, the third row of units in the heading indicates the magnetic field of the models in units of μG.
[a] Flux at the Earth, assuming the bow shock is a disk-shaped object with radius 0.″65. Flux in units 10^{-16} ergs cm^{-2} s^{-1}. Rest wavelengths of the emission lines are those in vacuum.

column of Table 3 and drawn schematically in Figure 8 lie somewhere between the 40 km s^{-1} magnetized shock model and the weakly magnetized 60 km s^{-1} shock model. Our composite model, denoted "60/40" in the next to last column of Table 3, matches the line ratios better than any single shock. In particular, strong low-excitation UV lines such as Mg II λ2800 and C II] λ2327 are understandable with the new model. The predicted fluxes in the Fe II UV bands match the observations, as well as any of the other lines; hence, abundances of Fe appear roughly solar within HH 47A. Abundances within other HH objects also appear to be roughly solar (Beck-Winchatz, Böhm, & Noriega-Crespo 1996).

The Balmer line ratios in the BS and MD are also consistent with a lower shock velocity in the BS than in the MD. The dereddened Balmer decrements (Hδ, Hγ, Hβ, Hα) in the MD and BS are the same except for Hα in the BS, which is observed to be 5.00 ± 0.23 brighter than Hβ, as opposed to the MD where it is 3.95 ± 0.14. That is, there is excess Hα emission in the BS as compared with the MD. Both ratios exceed recombination values ($\sim$3.0), as expected when collisional excitation is important, but the enhanced Balmer decrement in the BS suggests that collisions populate the lower excited states of H more there than they do in the MD, a process that affects the line ratios most in the lowest velocity shocks. As we discuss below, the BS also has more two-photon continuum than does the MD, even though the Hβ flux in the BS is fainter than that of the MD. These results again confirm that at least some of the shocks in the BS spectrum have a lower Mach number than that of the MD.

4.2. *The Blue Continuum Emission*

Both the BS and MD spectra show a distinct blue continuum in the optical that becomes quite strong in the ultraviolet. This blue continuum has been observed in HH 47A and other HH objects and is usually attributed to two-photon emission from the $n = 2$ level of H (Dopita et al. 1982; Schwartz 1983; Mor94), although a continuum peak near λ1580 may arise from H_2 fluorescence (Böhm, Scott, & Solf 1991).

The $2s\,S_{1/2}$ 2–$1s\,S_{1/2}$ 2 transition in H is strictly forbidden, but the atom can decay between these levels if it emits two photons whose total energy equals 10.2 eV. The maximum probability for this emission occurs if each photon has an energy of $\sim$5.1 eV, or λ2451. Although the photon number distribution N_ν peaks at λ2451, the spectral energy distribution $F_\nu \sim \nu N_\nu$ peaks at $\nu \sim 0.75\nu_{\mathrm{Ly}\alpha}$. The relationship $\nu F_\nu = \lambda F_\lambda$ shows that F_λ peaks at λ1422 for two-photon emission.

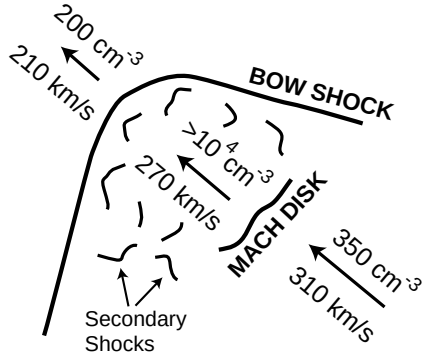

FIG. 8.—Schematic of the shock fronts in the HH 47A region. The velocities listed are with respect to the star. Fast jet gas overtakes the dense material within HH 47A at the Mach disk, and this dense material in turn overtakes slower jet material at the bow shock. Weak secondary shocks within the dense material should be strongly magnetized. The densities and velocities shown are for the "60/40" model described in the text.

Brugel et al. (1982) give an analytic approximation to the spectral energy distribution of two-photon emission. This analytic shape differs somewhat from one we calculated numerically (Table 4). Our solution is based on the probability distribution of two-photon emission given by Spitzer & Greenstein (1951). We fitted the N_ν distribution, which is symmetrical, with a ninth-order cubic spline and then converted this solution first to F_ν and then to F_λ. The values of $F_{\mathrm{TOT}}/\lambda F_\lambda$ in Table 4 are essentially bolometric corrections that can be used to convert an observed specific flux F_λ to the total flux in a two-photon spectrum. For example, if one measures the two-photon flux at λ5000 to be $F_\lambda = 1 \times 10^{-17}$ ergs cm^{-2} s^{-1} $Å^{-1}$, then $\lambda F_\lambda = 5 \times 10^{-14}$ ergs cm^{-2} s^{-1}, and from the bolometric correction of 7.50 in Table 3 we would infer a total energy flux in the two-photon continuum of 3.75×10^{-13} ergs cm^{-2} s^{-1}.

Analysis of this continuum has been a challenge because of the systematics noted in § 2. The continua measured from the dereddened spectra of the BS and MD using a number of spectral regions devoid of lines appear in Figure 2. After correcting for the larger dark counts at high geomagnetic latitudes (§ 2) and using $A_V = 0.30$ the bow shock and Mach disk continua match that expected from two-photon emission to within the uncertainties.

The MD continuum points scatter more than those of the BS because of the smaller integration time for the MD spectrum and because the continuum is particularly strong in the BS. The dereddened specific fluxes at λ3000 for the BS and MD are 2.2×10^{-17} and 1.7×10^{-17} ergs cm^{-2} s^{-1} $Å^{-1}$, respectively. According to Table 4, these specific fluxes imply total two-photon continuum fluxes of 1.6×10^{-13} ergs cm^{-2} s^{-1} for the BS and 1.2×10^{-13} ergs cm^{-2} s^{-1} for the MD. In terms of ratios with respect to Hβ = 100, the two-photon continuum of the BS is 18,000, whereas that for the MD is 10,800.

These fluxes show that two-photon emission is an important coolant in low-velocity shocks, having a flux between 20% and 50% of Lyα in the shock models compiled in Table 3. The stronger two-photon continuum in the BS spectrum is another indication that low-velocity shocks are present in the BS, as two-photon continuum increases relative to Hβ for low-velocity shocks (Table 3; Hartigan et al. 1987).

The models in Table 3 underestimate the two-photon continuum observed. We consider two potential explanations. It is possible that the models predict the right intrinsic two-photon emission but that Lyα photons are trapped and eventually converted to two-photon continuum. This process requires that the radiative decay rate divided by the number of scatterings be comparable to the rate of collisions from the $2p$ level of hydrogen to $2s$. Based on the densities quoted above and electron and proton collision rates from Janev et al. (1987), a Lyα photon would have to scatter 10^{10} times to be converted, requiring an H I column density of order 10^{21} cm^{-2}, larger than expected for the size and density of HH 47A. Another difficulty with the Lyα trapping hypothesis is that roughly a third of the Lyα photons are converted to molecular hydrogen fluorescent

TABLE 4

TWO-PHOTON SPECTRAL ENERGY DISTRIBUTION

λ (Å)	$F_\lambda/F_{1422\,Å}$	$F_{TOT}/\lambda F_\lambda$	λ (Å)	$F_\lambda/F_{1422\,Å}$	$F_{TOT}/\lambda F_\lambda$
1220.....	6.87 (−2)	12.8	1800	6.68 (−1)	0.89
1240.....	3.41 (−1)	2.54	1900	5.81 (−1)	0.97
1260.....	5.43 (−1)	1.57	2000	5.05 (−1)	1.07
1280.....	6.93 (−1)	1.21	2200	3.86 (−1)	1.27
1300.....	8.02 (−1)	1.03	2400	2.98 (−1)	1.50
1320.....	8.77 (−1)	0.93	2600	2.34 (−1)	1.77
1340.....	9.29 (−1)	0.86	2800	1.87 (−1)	2.05
1360.....	9.63 (−1)	0.82	3000	1.50 (−1)	2.39
1380.....	9.84 (−1)	0.79	3500	9.22 (−2)	3.33
1400.....	9.96 (−1)	0.77	4000	5.99 (−2)	4.49
1420.....	1.00	0.76	4500	4.07 (−2)	5.87
1440.....	9.98 (−1)	0.75	5000	2.87 (−2)	7.50
1460.....	9.91 (−1)	0.74	5500	2.08 (−2)	9.40
1480.....	9.79 (−1)	0.74	6000	1.55 (−2)	11.6
1500.....	9.65 (−1)	0.74	6500	1.18 (−2)	14.0
1520.....	9.49 (−1)	0.75	7000	9.14 (−3)	16.8
1540.....	9.31 (−1)	0.75	7500	7.20 (−3)	19.9
1560.....	9.12 (−1)	0.76	8000	5.75 (−3)	23.4
1600.....	8.71 (−1)	0.77	9000	3.81 (−3)	31.4
1640.....	8.29 (−1)	0.79	10000.....	2.62 (−3)	41.1
1680.....	7.87 (−1)	0.81	15000.....	6.05 (−4)	119
1720.....	7.46 (−1)	0.84	20000.....	2.26 (−4)	238
1760.....	7.06 (−1)	0.87			

emission (Curiel et al. 1995) and are not available for conversion to two-photon continuum.

The second explanation for the discrepancy between observed and predicted two-photon intensity is that the shock models do not adequately treat the hydrogen emission from slow shocks in neutral gas. The simplest extension of the models is to account for the lack of electron-ion temperature equilibration in the shock. Electrons are probably not efficiently heated in the shock (Schwartz et al. 1988; Laming et al. 1997). The effects could be quite severe for a shock in partially neutral gas because of the extremely effective cooling by Lyα (Ohtani 1980). However, we have run models assuming pure Coulomb collisional equilibration of electron and ion temperatures, and comparison with the fully equilibrated models in Table 3 shows changes of only a few percent in the intensity ratio of two-photon continuum to Hα. A more severe change to the model would be to drop the assumption that the electron distribution is Maxwellian. An individual electron diffuses in energy space under the influence of collisions. When it passes the Lyα excitation threshold of 10.2 eV, it is likely to lose all its energy by exciting Lyα, rather than gaining energy until it can excite Hα or Hβ. Comparison of the Coulomb collision timescale for a 10.5 eV electron (Spitzer 1978) with the lifetime between Lyα excitations suggests that departures from a Maxwellian will become substantial for ionization fractions of 20% or lower. These departures would primarily reduce the Hα and Hβ collisional excitation rates relative to those of the Lyα and the two-photon continuum.

5. CONCLUSIONS

In this paper we have analyzed high signal-to-noise optical and ultraviolet spectra of the bow shock and Mach disk within HH 47A taken with the FOS on *HST*. The new spectra cover the entire wavelength range from $\lambda\lambda$2200 to 6800. In addition to the bright Mg II and C II] lines expected in the mid-ultraviolet from a low-velocity shock, HH 47A also shows about a dozen distinct permitted Fe II lines in this wavelength region. An analysis of the energy levels and *A*-values of these Fe II lines shows several line ratios that are sensitive to the radiative transfer within the region. The observed ratios among these Fe II lines differ from those seen so far in other astronomical objects and are characteristic of a low-density plasma where resonant scattering dominates transitions to the ground level. Scattering optical depths measured directly from ratios of UV Fe II lines that originate from the same upper level can be achieved with the column densities and temperatures inferred from ratios of optical lines. Both the excitation and scattering of these Fe II lines occurs locally within the HH object. There is no evidence for significant depletion of Fe within HH 47A.

A blue continuum seen in both spectra in the optical extends into the ultraviolet and has a shape consistent with that expected for two-photon emission from hydrogen. We present a table of bolometric corrections for two-photon emission that can be used to measure the total luminosity in this continuum given a measurement of the specific flux at a single wavelength. The total two-photon fluxes we infer indicate that two-photon emission is an important coolant in the HH 47A shocks.

Shock models of the observed optical and ultraviolet line ratios indicate that secondary shocks within the cooling zone of the bow shock generate strong low-excitation lines and two-photon continua. These secondary shocks will be strongly magnetized because the B field is compressed within the postshock gas. The observed flux of the Balmer lines in the Mach disk translates directly into the mass flux of the jet through the Mach disk. The mass-loss rate at the position of the Mach disk is a factor of $\sim$20 lower than has been found closer to the star where the jet is brightest, an

indication of the episodic nature of the outflow. Our models allow us to estimate improved densities and shock velocities for both the bow shock and the Mach disk.

As has been the case with most objects that have been observed spectroscopically for the first time or with greater sensitivity in a new wavelength region, the mid-ultraviolet emission lines in HH 47A open up several new avenues of diagnostic possibilities, especially when combined with simultaneous optical spectroscopy. Deeper spectroscopic studies of HH objects, particularly at wavelengths shortward of $\lambda 2200$, hold great potential for similar emission-line studies. The two-photon continuum, H_2 continuum, reddening, and reddening law are also best studied at these shorter wavelengths, which should be accessible at good signal-to-noise ratio with the next generation of space-based instruments.

The authors would like to thank Chris Coco for his help in producing Figure 7, J. Weisheit for useful discussions on scattering, Ed Smith of STScI for his help and diligence in understanding the systematics of the FOS spectra, and Bo Reipurth for his comments on a draft of this paper.

REFERENCES

Allen, D. A. 1973, Astrophysical Quantities (London: Athlone), 31
Beck-Winchatz, B., Böhm, K. H., & Noriega-Crespo, A. 1996, AJ, 111, 346
Biro, S., & Raga, A. 1994, ApJ, 434, 221
Boggess, A., Bruhweiler, F. C., Grady, C. A., Ebbets, D. C., Kondo, Y., Trafton, L. M., Brandt, J. C., & Heap, S. R. 1991, ApJ, 377, L49
Böhm, K.-H., Bührke, Th., Raga, A. C., Brugel, E. W., Witt, A. N., & Mundt, R. 1987, ApJ, 316, 349
Böhm, K.-H., Scott, D. M., & Solf, J. 1991, ApJ, 371, 248
Böhm, K.-H., & Solf, J. 1990, ApJ, 348, 297
Brugel, E. W., Shull, J. M., & Seab, C. G. 1982, ApJ, 262, L35
Cardelli, J. A., Clayton, G. C., & Mathis, J. S. 1988, ApJ, 345, 245
Cheng, K.-P., Bruhweiler, F. C., & Neff, J. E. 1997, ApJ, 481, 866
Chevalier, R. A., Kirshner, R. P., & Raymond, J. C. 1980, ApJ, 235, 186
Chevalier, R. A., & Raymond, J. C. 1978, ApJ, 225, L27
Curiel, S., Raymond, J. C., Wolfire, M., Hartigan, P., Morse, J., Schwartz, R. D., & Nísenson, P. 1995, ApJ, 453, 322
Dopita, M. A. 1978, ApJS, 37, 117
Dopita, M. A., Binette, L., & Schwartz, R. D. 1982, ApJ, 261, 183
Dopita, M. A., Schwartz, R. D., & Evans, I. 1982, ApJ, 263, L73
Edwards, S., Mundt, R., & Ray, T. 1993, in Protostars and Planets III, ed. J. Lunine & E. H. Levy (Tucson: Univ. Arizona Press), 567
Eislöffel, J., Davis, C., Ray, T., & Mundt, R. 1994, ApJ, 422, L91
Eislöffel, J., & Mundt, R. 1994, A&A, 284, 530
Fawcett, B. C. 1988, Atomic Data and Nuclear Data Tables, Vol. 40, No. 1, p. 2
Graham, J., & Elias, J. 1983, ApJ, 272, 615
Hartigan, P. 1997, in ASP Conf. Ser. 121, Accretion Phenomena and Related Outflows, ed. D. T. Wickramasinghe, G. V. Bicknell, & L. Ferrario (San Francisco: ASP), 536
Hartigan, P., Edwards, S., & Ghandour, L. 1995, ApJ, 452, 736
Hartigan, P., Morse, J. A., & Raymond, J. 1994, ApJ, 436, 125 (HMR94)
Hartigan, P., Morse, J., Heathcote, S., Cecil, G., & Raymond, J. 1993, ApJ, 414, L121
Hartigan, P., & Raymond, J. 1993, ApJ, 409, 705
Hartigan, P., Raymond, J., & Hartmann, L. 1987, ApJ, 316, 323
Hartigan, P., Raymond, J., & Meaburn, J. 1990, ApJ, 362, 624
Hayes, J. E., & Lindner, D. J. 1996, The FOS Dark Count Rate, ISR-146 (Baltimore: STScI)
Heathcote, S., Morse, J., Hartigan, P., Reipurth, B., Schwartz, R. D., Bally, J., & Stone, J. 1996, AJ, 112, 1141
Janev, R. K., Langer, W. D., Evans, K., Jr., & Post, D. E., Jr. 1987, Elementary Processes in Hydrogen-Helium Plasmas (Berlin: Springer), 23, 133
Judge, P. G., & Jordan, C. 1991, ApJS, 77, 75
Keenan, F. P., Hibbert, A., Burke, P. G., & Berrington, K. A. 1988, ApJ, 332, 539
Laming, J. M., Raymond, J. C., McLaughlin, B. M., & Blair, W. P. 1997, ApJ, 472, 267
Longo, R., Stalio, R., Polidan, R. S., & Rossi, L. 1989, ApJ, 339, 474
Morse, J., Blair, W. P., & Raymond, J. 1999, Rev. Mexicana Astron. Astrofis., in press
Morse, J. A., Hartigan, P., Heathcote, S., Raymond, J. C., & Cecil, G. 1994, ApJ, 425, 738 (Mor94)
Nahar, S. N. 1995, A&A, 293, 967
Nahar, S. N., & Pradhan, A. K. 1994, J. Phys. B, 27, 429
Ohtani, H. 1980, PASJ, 32, 110
Penston, M. V., et al. 1983, MNRAS, 202, 833
Ray, T. P., Mundt, R., Dyson, J. E., Falle, S. A. E. G., & Raga, A. 1996, ApJ, 468, L103
Raymond, J. C. 1979, ApJS, 39, 1
Raymond, J. C., Blair, W. P., & Long, K. S. 1997, ApJ, 489, 314
Raymond, J. C., Blair, W. P., Long, K. S., Vancura, O., Edgar, R. J., Morse, J., Hartigan, P., & Sanders, W. T. 1997, ApJ, 482, 881
Raymond, J. C., Hartigan, P., & Hartmann, L. 1988, ApJ, 326, 323
Reipurth, B. 1989, in Low Mass Star Formation and Pre–Main-Sequence Objects, ed. B. Reipurth (Garching: ESO), 247
Reipurth, B., Bally, J., & Devine, D. 1997, AJ, 114, 2708
Reipurth, B., & Heathcote, S. 1991, A&A, 246, 511
Reipurth, B., Raga, A. C., & Heathcote, S. 1992, ApJ, 392, 145
Schwartz, R. D. 1983, ApJ, 268, L37
Schwartz, S. J., Thomsen, M. F., Bame, S. J., & Stansberry, J. 1988, J. Geophys. Res., 93, 12923
Shu, F. H., Najita, J., Ostriker, E., & Shang, H. 1995, ApJ, 455, L155
Spitzer, L., Jr. 1978, Physical Processes in the Interstellar Medium (New York: Wiley), 20
Spitzer, L., & Greenstein, J. 1951, ApJ, 114, 407
Stone, J. M., & Norman, M. L. 1993, ApJ, 413, 210
Szeifert, Th., Humphreys, R. M., Davidson, K., Jones, T. J., Stahl, O., Wolf, B., & Zickgraf, F.-J. 1996, A&A, 314, 131
Viotti, R., Rossi, L., Cassatella, A., Altamore, A., & Baratta, G. B. 1989, ApJS, 71, 983
Zickgraf, F.-J. 1988, in IAU Colloq. 94, Physics of Fe II Lines Outside of LTE, ed. R. Viotti et al. (Dordrecht: Reidel), 125